Available online at www.sciencedirect.com
ScienceDirect
Catalysis Today 117 (2006) 187–192
CATALYSIS TODAY
www.elsevier.com/locate/cattod

Synthesis and characterization of new promoters based on CeO_2–ZrO_2–Bi_2O_3 for automotive exhaust catalysts

Toshiyuki Masui, Keisuke Minami, Kazuhiko Koyabu, Nobuhito Imanaka *

Department of Applied Chemistry, Faculty of Engineering, Osaka University, 2-1 Yamadaoka, Suita, Osaka 565-0871, Japan

Available online 30 June 2006

Abstract

New oxidation catalysts based on CeO_2–ZrO_2–Bi_2O_3 solid solutions were synthesized for the effective oxidation of the soot particulates in the automotive emissions. Temperature programmed reduction and O_2 pulses experiments have been performed to examine the redox behavior of the CeO_2–ZrO_2–Bi_2O_3 catalysts. The CeO_2–ZrO_2–Bi_2O_3 solid solution showed both oxygen release below 300 °C and high oxygen storage capacity (OSC) over 1000 μmol O_2 g^{-1}, while those of the conventional CeO_2–ZrO_2 were 594 °C and 482 μmol O_2 g^{-1}, respectively. Furthermore, the low temperature reduction behavior of the CeO_2–ZrO_2–Bi_2O_3 solid solution was promoted by the addition of silver, which is an oxygen permeable component. The mechanism of the behavior was attributed to the synergetic effects of the partial solution of silver into the CeO_2–ZrO_2–Bi_2O_3 lattice and the surface deposition of silver on the solid solution. The reactivity of oxygen in the bulk of the catalyst greatly improves the soot combustion activities at low temperatures.

Keywords: Automotive exhasut catalyst; Temperature programmed reduction (TPR); Oxygen storage capacity (OSC); Raman spectroscopy; Soot combustion

1. Introduction

Oxygen-storage and -release properties of cerium oxide (CeO_2) play important roles in the field of oxidation catalysts, especially in the automotive catalytic converters [1–3]. CeO_2 and its related materials can lower the ignition temperatures of particulate matters (mainly soot) that are released from diesel vehicles [4]. Soot emission is a significant component of air pollution and is harmful for both human beings and the environment. In recent years, therefore, special attention has been paid to the synthesis and characterization of solid solutions based on CeO_2 for the cleaning of automotive emissions including diesel exhaust, because redox properties of the catalysts can contribute to lower the soot combustion temperature [5,6]. In particular, studies have focused on CeO_2–ZrO_2, which possess significantly enhanced thermal stability, redox property, and catalytic activities in comparison with those of pure CeO_2 [7–13].

Reduction behavior at low temperatures and high degree of reducibility of CeO_2–ZrO_2 solid solutions are significant properties in regards to automotive exhaust catalysts, because they correlate with the catalytic activity of the CeO_2-based catalysts [2]. The lowest reduction temperature and the highest degree of reducibility are typically considered as desirable properties [12]. Therefore, a number of investigations have been carried out to determine the optimal composition, structure, and morphology of the $Ce_xZr_{1-x}O_2$ solid solutions. Other studies have aimed at investigating the effect of trivalent dopants such as yttria [14–17], lanthana [14,15], and praseodymia [18] on the redox behavior of the $Ce_xZr_{1-x}O_2$ materials. However, it is difficult for such conventional materials to retain their reduction behavior at low temperatures after oxidation at high temperatures above 900 °C without alumina support. Although surface etching is known as one of the ways to solve this problem [19–21], this process is not a substantial improvement of the materials. Therefore, development of new promoters which show good redox property at low temperatures and high thermal stability has been required.

In this study, we propose the introduction of small amounts of Bi_2O_3 within the CeO_2–ZrO_2 lattice in order to promote the reduction of the $Ce_xZr_{1-x}O_2$ materials at low temperatures below 300 °C. The reasons why Bi_2O_3 is chosen as the third component are that (1) Bi_2O_3 and Bi_2O_3–Ln_2O_3 (Ln = Y, La–Yb) solid solutions show high oxide anion conductivity [22–

* Corresponding author. Tel.: +81 6 6879 7352; fax: +81 6 6879 7354.
E-mail address: imanaka@chem.eng.osaka-u.ac.jp (N. Imanaka).

0920-5861/$ – see front matter © 2006 Elsevier B.V. All rights reserved.
doi:10.1016/j.cattod.2006.05.015

Table 1
Composition, reduction temperature in TPR profiles, OSC, and BET specific surface area of the catalysts

Catalysts	Reduction temp. (°C)	OSC (μmol O_2 g^{-1})	BET surface area (m^2 g^{-1})
$Ce_{0.84}Zr_{0.16}O_{2.0}$	594 (1st run)	482 (1st run)	3.1
$Ce_{0.73}Zr_{0.17}Bi_{0.10}O_{1.95}$	250 (1st run), 384 (11th run)	647 (1st run), 709 (11th run)	2.9
$Ce_{0.68}Zr_{0.18}Bi_{0.14}O_{1.93}$	264 (1st run), 368 (11th run)	696 (1st run), 906 (11th run)	1.7
$Ce_{0.64}Zr_{0.16}Bi_{0.20}O_{1.9}$	316 (1st run), 344 (11th run)	1036 (1st run), 1004 (11th run)	0.8
$0.84Ce_{0.68}Zr_{0.18}Bi_{0.14}O_{1.93}$–0.16AgCl	336 (1st run), 344 (11th run)	951 (1st run), 732 (11th run)	1.3

26], (2) Bi_2O_3 is easily reduced to release oxygen [23], and (3) oxygen vacancies have to be produced within the lattice to keep charge balance because Bi^{3+} has lower valence (trivalent) than Ce^{4+} and Zr^{4+} (tetravalent). Furthermore, we have succeeded in retaining the low temperature reduction behavior by the addition of silver, which is well known as an oxygen-permeable material [27–30], into the CeO_2–ZrO_2–Bi_2O_3 solid solution.

2. Experimental

The CeO_2–ZrO_2–Bi_2O_3 solid solutions were prepared via co-precipitation. A mixture of 1 mol L^{-1} $Ce(NO_3)_3$, 1 mol L^{-1} $ZrO(NO_3)_2$, and 0.1 mol L^{-1} $Bi(NO_3)_3$ aqueous solutions was added dropwise into a 0.5 mol L^{-1} aqueous oxalic acid solution with stirring. The Ce:Zr:Bi molar ratio was set at 72:18:10, 68:17:15 and 64:16:20. The solution was adjusted to pH 3.2 by dropwise addition of 3 mol L^{-1} ammonia water. After stirring overnight, the precipitate was collected by filtration, then washed with deionized water several times and dried at 80 °C overnight. The dried powder was ground in an agate mortar and was calcined at 1000 °C in air for 1 h to obtain a CeO_2–ZrO_2–Bi_2O_3 solid solution. In addition, a binary CeO_2–ZrO_2 solid solution (Ce:Zr = 85:15) was also prepared by the same procedure for comparison.

Subsequently, one of the CeO_2–ZrO_2–Bi_2O_3 catalysts (Ce:Zr:Bi = 68:17:15) obtained by calcination was mixed with AgCl. The molar concentration of silver was 15 mol% in the mixture. The powders were ground and mixed by ball-milling treatment for 6 h, and the mixture was then calcined at 900 °C for 1 h to obtain a $0.85CeO_2$–ZrO_2–Bi_2O_3–0.15AgCl sample. The calcination temperature of the sample after AgCl addition was carried out at lower temperature by 100 °C than that before, because about half of AgCl is vaporized at 1000 °C.

The samples obtained were characterized using X-ray powder diffraction (XRD, Rigaku MultiFlex), X-ray fluorescence analysis (XRF, Rigaku ZSX100e) and Raman spectroscopy (Kaiser Optical Systems Inc., Holoprobe). Reduction behavior was studied using temperature-programmed reduction (TPR) in a pure hydrogen flow (80 mL min^{-1}) at a heating rate of 5 °C min^{-1} using a thermal conductivity detector of a gas chromatography instrument (Shimadzu, GC-8A). Oxygen storage capacity (OSC) was measured after the TPR measurement by a pulse injection method at 427 °C. Before the oxygen injection, the sample was outgassed under a helium flow. Pulses of oxygen (0.2 mL) were injected into the flow of helium passing through the sample until the breakthrough point was attained. The combustion temperature of soot (CABOT ELFTEX® 125, carbon black) was evaluated by thermogravimetric (TG) analysis using samples that contain 2 wt.% of soot in a flow of air (20 mL min^{-1}).

3. Results and discussion

X-ray fluorescence analyses were carried out on the CeO_2–ZrO_2–Bi_2O_3 materials, which was synthesized by a co-precipitation method, and on the AgCl-added CeO_2–ZrO_2–Bi_2O_3 sample, which was prepared by heating a ball-milled mixture of AgCl and CeO_2–ZrO_2–Bi_2O_3 obtained by co-precipitation. The sample composition of these catalysts determined by the X-ray fluorescent analysis was in good agreement with the theoretical value (within ± 1 mol%), which corresponds to the molar ratios of starting materials, as tabulated in Table 1.

Fig. 1 shows the X-ray powder diffraction patterns (XRD) of the catalysts. The $Ce_{0.86}Zr_{0.14}O_{2.0}$, $Ce_{0.73}Zr_{0.17}Bi_{0.10}O_{1.95}$, $Ce_{0.68}Zr_{0.18}Bi_{0.14}O_{1.93}$, and $Ce_{0.64}Zr_{0.16}Bi_{0.20}O_{1.9}$ catalysts displayed only diffraction peaks that are attributable to a cubic fluorite-type structure, whereas the diffraction pattern for the AgCl-added sample exhibited a small amount of the AgCl phase as a secondary phase.

In the XRD patterns of $Ce_{0.86}Zr_{0.14}O_{2.0}$ (Fig. 1(a)) and three CeO_2–ZrO_2–Bi_2O_3 samples (Fig. 1(b)–(d)), all diffraction peaks shifted to higher angles with increasing the Bi^{3+} content, suggesting that Bi^{3+} dissolves into the CeO_2–ZrO_2 lattice to form solid solutions. On the contrary, $0.84Ce_{0.68}Zr_{0.18}Bi_{0.14}O_{1.93}$–

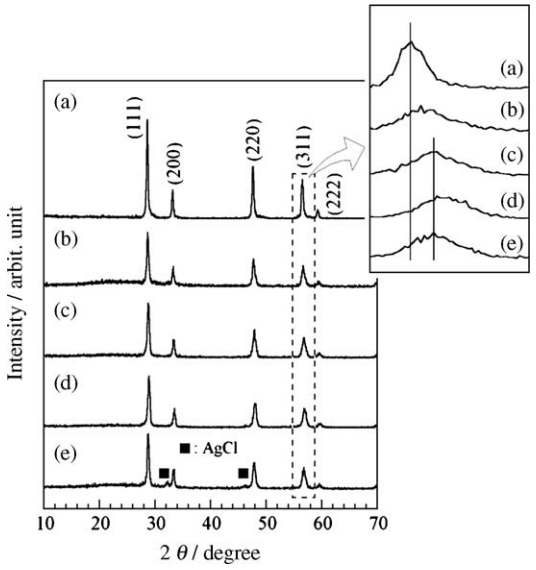

Fig. 1. X-ray powder diffraction patterns of the catalysts: (a) $Ce_{0.86}Zr_{0.14}O_{2.0}$, (b) $Ce_{0.73}Zr_{0.17}Bi_{0.10}O_{1.95}$, (c) $Ce_{0.68}Zr_{0.18}Bi_{0.14}O_{1.93}$, (d) $Ce_{0.64}Zr_{0.16}Bi_{0.20}O_{1.9}$, and (e) $0.84Ce_{0.68}Zr_{0.18}Bi_{0.14}O_{1.93}$–0.16AgCl.

0.16AgCl was identified as a simple mixture of $Ce_{0.68}Zr_{0.18}Bi_{0.14}O_{1.93}$ and AgCl, because the diffraction angles for the fluorite peaks of $Ce_{0.68}Zr_{0.18}Bi_{0.14}O_{1.93}$ (Fig. 1(c)) are coincided with those of $0.84Ce_{0.68}Zr_{0.18}Bi_{0.14}O_{1.93}$–16AgCl (Fig. 1(e)). The lattice parameters calculated from the XRD patterns calibrated with α-alumina were 0.5373 nm for $Ce_{0.86}Zr_{0.14}O_{2.0}$, 0.5387 nm for $Ce_{0.73}Zr_{0.17}Bi_{0.10}O_{1.95}$, 0.5379 nm for $Ce_{0.68}Zr_{0.18}Bi_{0.14}O_{1.93}$, 0.5402 nm for $Ce_{0.64}Zr_{0.16}Bi_{0.20}O_{1.9}$, and 0.5376 nm for $0.84Ce_{0.68}Zr_{0.18}Bi_{0.14}O_{1.93}$–0.16AgCl, respectively.

Reduction temperature and OSC value of the $Ce_{0.86}Zr_{0.14}O_{2.0}$, $Ce_{0.73}Zr_{0.17}Bi_{0.10}O_{1.95}$, $Ce_{0.68}Zr_{0.18}Bi_{0.14}O_{1.93}$, and $Ce_{0.64}Zr_{0.16}Bi_{0.20}O_{1.9}$ samples were determined from the TPR profiles (Fig. 2) and the subsequent O_2 pulse injection as summarized with BET specific surface area in Table 1. Although the reduction temperature and OSC increased with the increase in the amount of Bi^{3+} content, all CeO_2–ZrO_2–Bi_2O_3 catalysts were reduced at considerably lower temperatures (250–316 °C) than that of $Ce_{0.86}Zr_{0.14}O_{2.0}$ (594 °C). Furthermore, OSC of the $Ce_{0.64}Zr_{0.16}Bi_{0.20}O_{1.9}$ catalyst (1036 μmol O_2 g^{-1}) was more than twice that of the conventional $Ce_{0.86}Zr_{0.14}O_{2.0}$ material (482 μmol O_2 g^{-1}). The reason for such characteristics was that Bi_2O_3 was reduced to metallic Bi easily and that both Ce^{4+} and Bi^{3+} were reduced simultaneously [31].

However, the reduction temperature of the CeO_2–ZrO_2–Bi_2O_3 catalysts increased when the reduction and re-oxidation process was repeated 10 times at 900 °C (redox aging process), as evidenced in the 11th run of the TPR profiles in all samples. For example, the initial temperature-programmed reduction (TPR) trace of $Ce_{0.68}Zr_{0.18}Bi_{0.14}O_{1.93}$ displayed a reduction peak at 264 °C (Fig. 2(d)), but the significant upward shift in temperature of the main reduction peak, relative to the profile of the as-prepared sample, was observed after ten cycles of redox aging (Fig. 2(e)). This behavior implies that the reducibility of the sample has been deteriorated considerably.

In order to avoid such deterioration, we have developed a new material which can retain the low temperature activities by adding an oxygen permeable component, silver, to the $Ce_{0.68}Zr_{0.18}Bi_{0.14}O_{1.93}$ solid solution [32], because it is expected to promote the reduction of the sample. TPR curves of the as-prepared (1st run) and the redox-aged (11th run) $0.84Ce_{0.68}Zr_{0.18}Bi_{0.14}O_{1.93}$–0.16AgCl catalysts are shown in Fig. 3. The initial TPR trace of $0.84Ce_{0.68}Zr_{0.18}Bi_{0.14}O_{1.93}$–0.16AgCl (1st run, Fig. 3(a)) indicated a reduction behavior at around 340 °C, which was slightly higher than that of the $Ce_{0.68}Zr_{0.18}Bi_{0.14}O_{1.93}$. In contrast to the results observed in the CeO_2–ZrO_2–Bi_2O_3 catalysts, however, this reduction behavior was unaffected by 10 cycles of the redox aging process (11th run, Fig. 3(b)). The OSC values of the as-prepared and the aged $0.84Ce_{0.68}Zr_{0.18}Bi_{0.14}O_{1.93}$–0.16AgCl samples were 951 and 732 μmol O_2 g^{-1}, respectively.

In order to identify the origin of the different reduction behaviors described above, Raman spectra of the catalysts were measured as depicted in Fig. 4. The Raman spectrum of $Ce_{0.68}Zr_{0.18}Bi_{0.14}O_{1.93}$ exhibited a strong band at 467 cm^{-1}, which was assigned to the F_{2g} mode of a cubic fluorite structure, and two minor peaks at 313 and 573 cm^{-1} corresponding to B_{1g} and A_{1g} modes of the partially stabilized tetragonal zirconia structure, respectively. Such spectral features are indicative of a t″ phase, which is a type of a tetragonal structure containing oxygen displacement within the

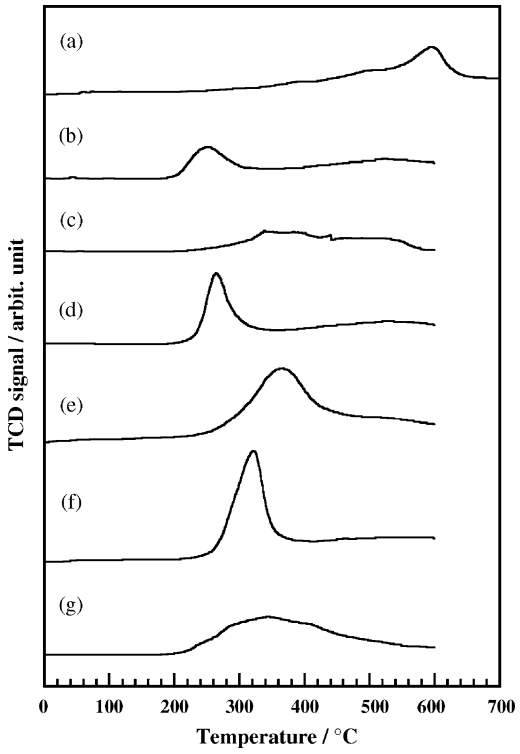

Fig. 2. Temperature programmed reduction profiles of the CeO_2–ZrO_2–Bi_2O_3 catalysts: (a) as-prepared $Ce_{0.86}Zr_{0.14}O_{2.0}$, (b) as-prepared $Ce_{0.73}Zr_{0.17}Bi_{0.10}O_{1.95}$ (1st run), (c) $Ce_{0.73}Zr_{0.17}Bi_{0.10}O_{1.95}$ after 10 cycles of reduction and subsequent re-oxidation treatment (11th run), (d) as-prepared $Ce_{0.68}Zr_{0.18}Bi_{0.14}O_{1.93}$ (1st run), (e) $Ce_{0.68}Zr_{0.18}Bi_{0.14}O_{1.93}$ after 10 cycles of reduction and subsequent re-oxidation treatment (11th run), (f) as-prepared $Ce_{0.64}Zr_{0.16}Bi_{0.20}O_{1.9}$ (1st run), and (g) $Ce_{0.64}Zr_{0.16}Bi_{0.20}O_{1.9}$ after 10 cycles of reduction and subsequent re-oxidation treatment (11th run).

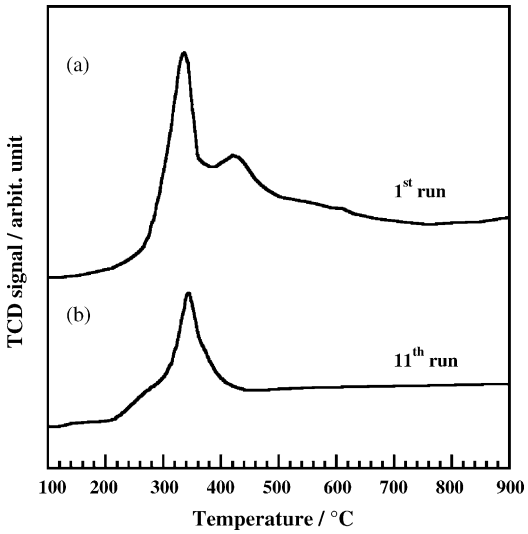

Fig. 3. Temperature programmed reduction profiles of the CeO_2–ZrO_2–Bi_2O_3–AgCl catalyst: (a) as-prepared $0.84Ce_{0.68}Zr_{0.18}Bi_{0.14}O_{1.93}$–0.16AgCl (1st run) and (b) $0.84Ce_{0.68}Zr_{0.18}Bi_{0.14}O_{1.93}$–0.16AgCl after 10 cycles of reduction and subsequent re-oxidation treatment (11th run).

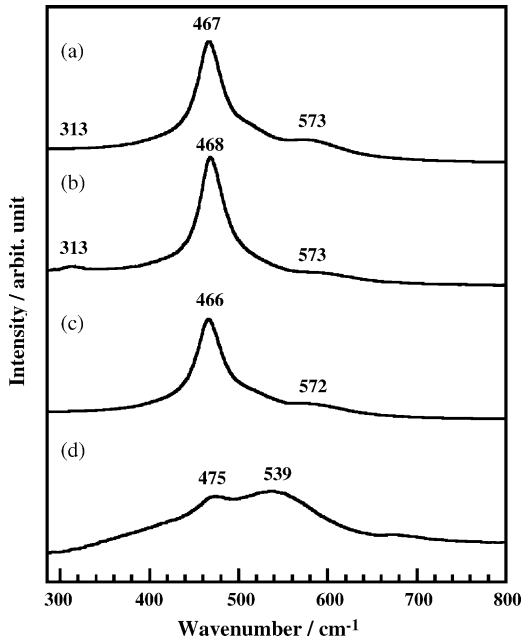

Fig. 4. Raman spectra of the $Ce_{0.68}Zr_{0.18}Bi_{0.14}O_{1.93}$ and the $0.84Ce_{0.68}Zr_{0.18}Bi_{0.14}O_{1.93}$–0.16AgCl catalysts: (a) as-prepared $Ce_{0.68}Zr_{0.18}Bi_{0.14}O_{1.93}$, (b) $Ce_{0.68}Zr_{0.18}Bi_{0.14}O_{1.93}$ after 10 cycles of reduction and subsequent re-oxidation treatment, (c) as-prepared $0.84Ce_{0.68}Zr_{0.18}Bi_{0.14}O_{1.93}$–0.16AgCl, and (d) $0.84Ce_{0.68}Zr_{0.18}Bi_{0.14}O_{1.93}$–0.16AgCl after 10 cycles of reduction and subsequent re-oxidation treatment.

fluorite lattice [33]. Although the Raman profile was not affected by the redox aging, a small amount of Bi_2O_3 deposition was detected in the XRD pattern, as shown in Fig. 5(a). This deposition induced the decreasing of Bi content in the catalysts on account of vaporization of metallic bismuth produced by the reduction of Bi_2O_3, because the melting point of metallic Bi is 271.3 °C. Indeed, vaporization of Bi after ten cycles of redox aging results in a 4% decrease in the amount of Bi in the sample. The decreasing of Bi content in the solid solution will be

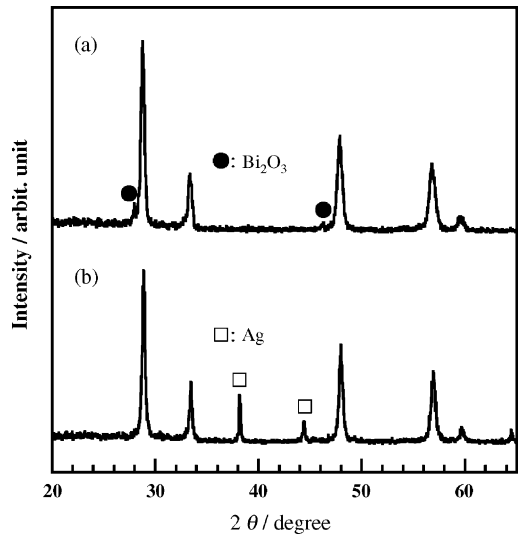

Fig. 5. XRD patterns of the catalysts after 10 cycles of reduction and subsequent re-oxidation treatment: (a) $Ce_{0.68}Zr_{0.18}Bi_{0.14}O_{1.93}$ and (b) $0.84Ce_{0.68}Zr_{0.18}Bi_{0.14}O_{1.93}$–0.16AgCl.

resposndibe for the deterioration of the reducibility, that is, the rise of the reduction temperature.

On the other hand, the Raman spectrum of $0.84Ce_{0.68}Zr_{0.18}Bi_{0.14}O_{1.93}$–0.16AgCl exhibited a remarkable behavior. After 10 cycles of redox aging, a new strong broad band corresponding to the Ag–O vibration [34,35] appeared at 539 cm^{-1}. This suggests that a part of silver ions can dissolve into the $Ce_{0.68}Zr_{0.18}Bi_{0.14}O_{1.93}$ lattice. Since the reoxidation process carried out at 427 °C, which was above the decomposition temperatures of AgO (100 °C) and Ag_2O (400 °C) [28], the Ag–O band at 539 cm^{-1} should not be observed if Ag did not dissolve into the $Ce_{0.68}Zr_{0.18}Bi_{0.14}O_{1.93}$ lattice. The partial dissolution of silver ions into the $Ce_{0.68}Zr_{0.18}Bi_{0.14}O_{1.93}$ lattice produces oxide anion vacancies to keep charge balance. The vacancies will contribute to the oxide anion mobility, which results in the retention of the low temperature reduction around 340 °C. However, the oxygen storage capacity decreased from 951 to 732 μmol O_2 g^{-1} by the dissolution of silver ions because of the decrease in the total amount of oxide anions in the lattice.

Furthermore, the XRD pattern of the redox treated $0.84Ce_{0.68}Zr_{0.18}Bi_{0.14}O_{1.93}$–0.16AgCl suggests surface deposition of metallic silver (Fig. 5(b)), because the melting point of AgCl is 455 °C and the liquid AgCl was impregnated on the surface of $Ce_{0.68}Zr_{0.18}Bi_{0.14}O_{1.93}$. The lattice parameter of the fluorite phase slightly decreased from 0.5379 to 0.5365 nm after the redox aging, which was probably due to both the Ag dissolution and the loss of Bi. The AgCl component in the $0.84Ce_{0.68}Zr_{0.18}Bi_{0.14}O_{1.93}$–0.16AgCl sample was reduced to metallic Ag by the initial reduction process in the TPR measurement. No chroline was detedced by the X-ray fluorescent analysis after the end both of the initial and the 11th redox cycles.

In contrast to the results for $Ce_{0.68}Zr_{0.18}Bi_{0.14}O_{1.93}$ (Fig. 5(a)), no phase separation to form Bi_2O_3 was observed in $0.84Ce_{0.68}Zr_{0.18}Bi_{0.14}O_{1.93}$–0.16AgCl and the decreasing percentage of Bi after ten cycles of redox aging was only 0.8%. An alloying effect between Ag and Bi is suggested for the suppression of Bi vaporization, because metallic silver can react with bismuth to form Ag–Bi alloys under reducing conditions and the melting points of the alloys are higher than 800 °C in the region of Ag > 80%) [36]. Accordingly, the retention of the low temperature reduction behavior of $0.84Ce_{0.68}Zr_{0.18}Bi_{0.14}O_{1.93}$–0.16AgCl could be attributed to the synergetic effects of partial dissolution of silver into the $Ce_{0.68}Zr_{0.18}Bi_{0.14}O_{1.93}$ lattice to form a substitutional solid solution and the surface deposition of metallic silver, which can prevent the vaporization by alloying to form Ag–Bi alloys.

The oxidation activity of the catalysts was examined from the standpoint of their ability to lower the combustion temperature of soot, which is in the range of 450–600 °C in the absence of the catalysts [4]. Thermogravimetric (TG) curves for soot combustion in the presence and the absence of the oxide catalysts are shown in Fig. 6. The weight loss on the TG curves indicates the combustion of soot particulates.

Our results indicate good correlation between the weight loss and the reactivity of the bulk oxygen of the catalyst. The

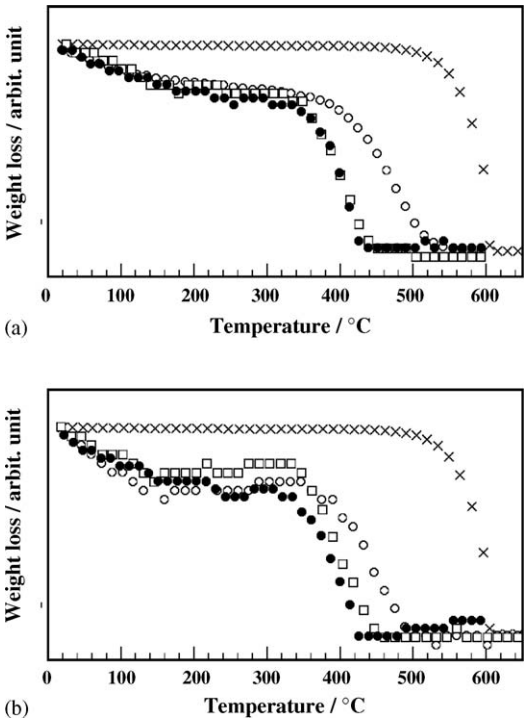

Fig. 6. Thermogravimetric analysis curves of carbon black combustion for $Ce_{0.86}Zr_{0.14}O_{2.0}$ (○), $Ce_{0.68}Zr_{0.18}Bi_{0.14}O_{1.93}$ (□) and $0.84Ce_{0.68}Zr_{0.18}Bi_{0.14}O_{1.93}$–0.16AgCl (●) catalysts: (a) as-prepared samples and (b) aged samples after 10 cycles of the reduction and subsequent re-oxidation treatment. The symbol (×) corresponds to the result for the combustion of carbon black itself in the absence of the catalysts.

soot oxidation temperature of the $Ce_{0.68}Zr_{0.18}Bi_{0.14}O_{1.93}$ and the $0.84Ce_{0.68}Zr_{0.18}Bi_{0.14}O_{1.93}$–0.16AgCl catalysts was appreciably lower than that of the conventional CeO_2–ZrO_2. Because the reduction temperatures of the initial $Ce_{0.68}Zr_{0.18}Bi_{0.14}O_{1.93}$ and $0.84Ce_{0.68}Zr_{0.18}Bi_{0.14}O_{1.93}$–0.16AgCl catalysts are comparable, combustion of soot occurs at the same temperature (Fig. 6(a)). However, differences in the combustion temperatures were observed after ten cycles of redox aging (Fig. 6(b)). The soot combustion temperature for the $Ce_{0.68}Zr_{0.18}Bi_{0.14}O_{1.93}$ catalyst increased slightly, because of the higher temperature at which the active oxygen was released from this sample by the redox aging. As demonstrated in Fig. 6, the active oxygen released from the catalyst correlates with soot oxidation, and the reactivity highly improves the soot combustion activities.

4. Conclusions

Reduction temperature of the CeO_2–ZrO_2 catalysts decreased remarkably by the doping of bismuth oxide into the lattice to form ternary solid solutions. The CeO_2–ZrO_2–Bi_2O_3 solid solutions can store a larger amount of oxygen at low temperatures than the conventional CeO_2–ZrO_2 catalyst. The soot oxidation temperature of the CeO_2–ZrO_2–Bi_2O_3 catalysts appreciably decreased in comparison with the conventional CeO_2–ZrO_2, because active oxygen molecules can be released from the bulk at lower temperatures.

Furthermore, retention of low temperature reduction behavior of CeO_2–ZrO_2–Bi_2O_3 was realized by the addition of silver to the solid solution. Based on our results, it can be suggested that the synergistic effects of the partial solution and surface deposition of silver are responsible for maintaining the activity, in which the oxygen permeability of silver enhances low temperature reduction, even after ten cycles of redox aging.

Acknowledgements

The authors sincerely thank Dr. Kuniaki Murase and Prof. Yasuhiro Awakura (Kyoto University) for their assistance with the Raman spectra measurements. The present work was supported by a Grant-in-Aid for Scientific Research No. 17350100 from Japan Society for the Promotion of Science (JSPS). This work was also partially supported by the Industrial Technology Research Grant Program in 02 (Project No. 02A27004c) from the New Energy and Industrial Technology Development Organization (NEDO) based on funds provided by the Ministry of Economy, Trade and Industry, Japan (METI).

References

[1] J. Kašpar, P. Fornasiero, N. Hickey, Catal. Today 77 (2003) 419.
[2] J. Kašpar, P. Fornasiero, M. Graziani, Catal. Today 50 (1999) 285.
[3] A. Trovarelli (Ed.), Catalysis by Ceria and Related Materials, Imperial College Press, London, 2002.
[4] J.F. Lamonier, S.P. Kulyova, E.A. Zhikinskaya, B.G. Kostyuk, V.V. Lumin, A. Aboukaïs, Kinet. Catal. 45 (2004) 429.
[5] G. Neri, G. Rizzo, S. Galvagno, M.G. Musolini, A. Donato, R. Pietropaolo, Thermochim. Acta 381 (2002) 165.
[6] E. Aneggi, M. Boaro, C. de Leitenberg, G. Dolcetti, A. Trovarelli, J. Alloys Compd. 408–412 (2006) 1096.
[7] M. Ozawa, M. Kimura, A. Isogai, J. Alloys Compd. 193 (1993) 73.
[8] A. Trovarelli, C. de Leirenburg, G. Dolcetti, Chemtech 27 (1997) 32.
[9] M. Ozawa, J. Alloys Compd. 275–277 (1998) 886.
[10] M. Sugiura, Catal. Suv. Asia. 7 (2003) 77.
[11] J. Kašpar, P. Fornasiero, J. Solid State Chem. 171 (2003) 19.
[12] R. Di Monte, J. Kašpar, Catal. Today 100 (2005) 27.
[13] R. Di Monte, J. Kašpar, J. Mater Chem. 15 (2005) 633.
[14] P. Vidmar, P. Fornasiero, J. Kašpar, G. Gubitosa, M. Graziani, J. Catal. 171 (1997) 160.
[15] L.N. Ikryannikova, A.A. Aksenov, G.L. Markaryan, G.P. Muravieva, B.G. Kostyuk, A.N. Kharlanov, E.V. Lunina, Appl. Catal. A 210 (2001) 225.
[16] G.L. Markaryan, L.N. Ikryannikova, G.P. Muravieva, A.O. Turakulova, B.G. Kostyuk, E.V. Lunina, V.V. Lunin, E. Zhilinskaya, A. Aboukais, Colloids Surf. A 151 (1999) 435.
[17] T. Settu, R. Gobinathan, J. Eur. Ceram. Soc. 16 (1996) 1309.
[18] C.K. Narula, L.P. Haack, W. Chun, H.-W. Jen, G.W. Graham, J. Phys. Chem. B 103 (1999) 3634.
[19] T. Masui, K. Nakano, T. Ozaki, G. Adachi, Z. Kang, L. Eyring, Chem. Mater. 13 (2001) 1834.
[20] T. Ozaki, T. Masui, K. Machida, G. Adachi, T. Sakata, H. Mori, Chem. Mater. 12 (2000) 643.
[21] J. Kašpar, R. Di Monte, P. Fornasiero, M. Graziani, H. Bradshaw, C. Norman, Top. Catal. 16–17 (2001) 83.
[22] P. Shuk, H.-D. Wiemhöfer, U. Guth, W. Göpel, M. Greenblatt, Soild State Ionics 89 (1996) 179.
[23] M.G. Hapase, V.B. Tare, A.B. Biswas, Ind. J. Pure Appl. Phys. 5 (1967) 401.
[24] T. Takahashi, H. Iwahara, Mater. Res. Bull. 13 (1978) 1447.

[25] H. Iwahara, T. Esaka, T. Sato, T. Takahashi, J. Solid State Chem. 39 (1981) 173.
[26] S. Dikmen, P. Shuk, M. Greenblatt, Soild State Ionics 112 (1998) 299.
[27] L.C. Beavis, Rev. Sci. Instrum. 43 (1972) 122.
[28] J.F. Weaver, G.B. Hoflund, J. Phys. Chem. 98 (1994) 8519.
[29] R.A. Outlaw, S.N. Sankaran, G.B. Hoflund, M.R. Davidson, J. Mater. Res. 3 (1988) 1378.
[30] R.A. Outlaw, D. Wu, G.B. Hoflund, M.R. Davidson, J. Vac. Sci. Technol. A 10 (1992) 1497.
[31] K. Minami, T. Masui, N. Imanaka, L. Dai, B. Pacaud, J. Alloys Compd. 408–412 (2006) 1132.
[32] N. Imanaka, T. Masui, K. Minami, K. Koyabu, Chem. Mater. 17 (2005) 6511.
[33] M. Yashima, H. Arashi, M. Kakihana, M. Yoshimura, J. Am. Ceram. Soc. 77 (1994) 1067.
[34] G.J. Millar, M.L. Nelson, P.J.R. Uwins, Catal. Lett. 43 (1997) 97.
[35] G.I.N. Waterhouse, G.A. Bowmaker, J.B. Metson, Phys. Chem. Chem. Phys. 3 (2001) 3838.
[36] I. Karakaya, W.T. Thompson, J. Phase Equil. 14 (1993) 525.